Final Report

Project Title:	Advanced Nanomaterials for High-Efficiency Solar Cells
Covering Period:	Sept. 1, 2010 to Aug. 31, 2013
Date of Report:	Nov. 29, 2013
Recipient:	University of Wisconsin-Milwaukee
Award Number:	DE-EE0003208
Working Partners:	None
Cost-Sharing Partners:	UW-Milwaukee and We Energies

Contacts:

Junhong Chen
Department of Mechanical Engineering
University of Wisconsin-Milwaukee
3200 N Cramer Street
Milwaukee, WI 53211
Phone: 414-229-2615
E-mail: jhchen@uwm.edu

DOE Project Team:	DOE Field Contracting Officer	-	Lalida Crawford
	DOE Field Project Officer	-	Steven Palmeri
	DOE Grants & Agreements Specialist	-	Diana Heyder
	Project Monitor	-	Andrew Kobusch

Executive Summary

Energy supply has arguably become one of the most important problems facing humankind. The exponential demand for energy is evidenced by dwindling fossil fuel supplies and record-high oil and gas prices due to global population growth and economic development. This energy shortage has significant implications to the future of our society, in addition to the greenhouse gas emission burden due to consumption of fossil fuels. Solar energy seems to be the most viable choice to meet our clean energy demand given its large scale and clean/renewable nature. However, existing methods to convert sun light into electricity are not efficient enough to become a practical alternative to fossil fuels.

This DOE project aims to develop advanced hybrid nanomaterials consisting of semiconductor nanoparticles (quantum dots or QDs) supported on graphene for cost-effective solar cells with improved conversion efficiency for harvesting abundant, renewable, clean solar energy to relieve our global energy challenge. Expected outcomes of the project include new methods for low-cost manufacturing of hybrid nanostructures, systematic understanding of their properties that can be tailored for desired applications, and novel photovoltaic cells.

Through this project, we have successfully synthesized a number of novel nanomaterials, including vertically-oriented graphene (VG) sheets, three-dimensional (3D) carbon nanostructures comprising few-layer graphene (FLG) sheets inherently connected with CNTs through sp^2 carbons, crumpled graphene (CG)-nanocrystal hybrids, CdSe nanoparticles (NPs), CdS NPs, nanohybrids of metal nitride decorated on nitrogen-doped graphene (NG), QD-carbon nanotube (CNT) and QD-VG-CNT structures, TiO_2-CdS NPs, and reduced graphene oxide (RGO)-SnO_2 NPs. We further assembled CdSe NPs onto graphene sheets and investigated physical and electronic interactions between CdSe NPs and the graphene. Finally we have demonstrated various applications of these nanomaterials in solar cells (both as photoanodes and counter electrodes), gas sensors, and energy storage devices. This research is potentially transformative since the availability of affordable hybrid nanostructures and their fundamental properties will enable various innovative applications of the multifunctional hybrid nanostructures and thus will accelerate new discoveries and inventions in nanoscience and nanotechnology.

Project Objective:

This project aims to develop advanced hybrid nanomaterials consisting of semiconductor nanoparticles (quantum dots or QDs) supported on graphene for cost-effective solar cells with improved conversion efficiency for harvesting abundant, renewable, clean solar energy to relieve our global energy challenge. Expected outcomes of the project include new methods for low-cost manufacturing of hybrid nanostructures, systematic understanding of their properties that can be tailored for desired applications, and novel photovoltaic cells.

Background:

Energy supply has arguably become one of the most important problems facing humankind. The exponential demand for energy is evidenced by dwindling fossil fuel supplies and record-high oil and gas prices due to global population growth and economic development. This energy shortage has significant implications to the future of our society. For example, in order for 10 billion people to sustain their current lifestyle with their current energy consumption, we need a minimum of ten additional terawatts (TW) until the year 2050. The energy crisis is further exacerbated by major concerns about global warming from greenhouse gas emissions due to increasing fossil fuel consumption.

At this large scale, solar energy seems to be the most viable choice to meet our clean energy demand. The sun continuously delivers to the Earth 120,000 TW of energy, which dramatically exceeds our current rate of energy needs (13 TW). However, existing methods to convert sun light into electricity are not efficient enough to become a practical alternative to fossil fuels. The best commercial solar cells based on single-crystal silicon are about 18% efficient. These conventional p-n junction cells suffer from the high cost of manufacturing and installation. Excitonic solar cells, such as bulk heterojunction cells, dye-sensitized solar cells (DSSCs), and organic cells, are promising for inexpensive and large-scale solar energy conversion. Laboratory DSSCs based on cheap dye sensitization of oxide semiconductors are typically less than 10% efficient, and those based on even cheaper organic materials are 2-5% efficient. Although the DSSC has been identified as the most efficient and stable cells, its efficiency is limited by the electron transport across semiconductor particle film that is susceptible for recombination loss at grain boundaries. One research trend to further improve the cell efficiency is the use of nanostructures to facilitate electron transport. Ordered 1-D arrays of ZnO nanowires and nanotubes have been demonstrated as the backbone of electron transport. Recently, carbon nanotubes (CNTs) have been shown to significantly facilitate the electron transport and enhance the cell efficiency. A second research trend in this area is the use of QDs to replace the organic dyes. QDs provide several significant advantages over dyes. The use of QDs allows for the tuning of optical absorption through the selection of QD materials and sizes. It could also potentially take advantage of the recently observed multiple electron-hole pair generation per photon to achieve a higher cell efficiency than the limit predicted by Shockley and Queisser.

The overall research objectives of this project are to advance the manufacture and the fundamental understanding of hybrid nanoparticle-graphene structures and to

develop hybrid-nanostructure-based photovoltaic cells for converting solar energy to electricity. The study will be based on the PI's recent success in the controlled assembly of nanoparticles onto the CNT surface and graphene sheets and in the fabrication of novel electronic devices using hybrid nanostructures. This research is potentially transformative since the availability of affordable hybrid nanostructures and their fundamental properties will enable various innovative applications of the multifunctional hybrid nanostructures and thus will accelerate new discoveries and inventions in nanoscience and nanotechnology.

Major Activities and Results:

We have successfully synthesized reduced graphene oxide (RGO) sheets in solution, vertically-oriented graphene (VG) sheets in the gas phase, aerosol CdSe nanoparticles (NPs) (**Fig. 1**), and colloidal CdSe NPs (**Fig. 2**). We further assembled CdSe NPs onto graphene sheets and investigated physical and electronic interactions between CdSe NPs and the graphene (**Fig. 3**). The resulting hybrid nanostructure exhibited photoresponse to both laser and simulated sunlight AM 1.5G excitation (**Fig. 4**). The hybrid structure with low CdSe NP coverage showed distinct photoresponse times in air, N2, NH3, and NO2, while high CdSe NP coverage led to nearly constant but three orders of magnitude smaller response time in all gases (**Fig. 5**). Such a difference in photoresponse as a function of NP coverage is attributed to the energy band bending at the interface between the RGO and the CdSe NP. We have produced a brand-new, three-dimensional (3D) carbon nanostructure comprising few-layer graphene (FLG) sheets inherently connected with CNTs through sp^2 carbons, resembling plant leaves (FLGs) growing on stems (CNTs) (**Fig. 6**). The new 3D carbon nanostructure is attractive for various electronic and optoelectronic applications. We have also acquired a set of solar cell characterization equipment for subsequent measurements.

We have demonstrated a facile and versatile route to synthesize nanohybrids of metal nitride decorated on nitrogen-doped graphene (NG) (**Figs. 7&8**). The TiN/NG nanohybrids can be used as a low-cost counter electrode to replace Pt in DSSCs (**Fig. 9**). We have also synthesized vertically-oriented graphene (VG) nanosheets for counter electrodes (CEs) of dye-sensitized solar cells (DSSCs) using a PECVD process (**Fig. 10**). Increasing water vapor concentration in the synthesis can decrease the charge transfer resistance of VG electrodes to as low as 1% of that of Pt electrodes (**Fig. 11**). The enhanced catalytic performance can be attributed to a large accessible surface area, a hierarchical structure, and abundant oxygen functional groups of VG (**Fig. 12**). DFT calculations reveal that the oxygen functional groups, especially epoxide groups, are crucial for the triiodide reduction (**Fig. 13**). Through optimizing the VG CEs, a PCE of 5.36% has been achieved, which is higher than that of DSSCs with Pt electrode (4.68%) (**Fig. 14**). Finally, we have fabricated and characterized solar cells using photoanodes consisting of QD-CNT and QD-VG-CNT structures (**Fig. 15**). The QD-VG-CNT solar cell displayed a higher power conversion efficiency (PCE), about 5-fold higher than the QD-CNT solar cell, which suggests that the addition of VG significantly improves the solar cell performance (**Fig. 16**). We further demonstrated a CdS QD-sensitized solar cell with significantly enhanced stability and depressed recombination in I^-/I^{3-} electrolyte (**Fig. 17**). The CdS QDs were deposited in a mesoporous TiO_2 film

using chemical bath deposition. Following the coating of an ultrathin TiO_2 protection layer using atomic layer deposition (ALD), the performance and stability of CdS QD sensitized solar cells were pronouncedly enhanced (**Figs. 18&19**).

Quantum dots (QDs) and dye co-sensitized solar cells have attracted substantial interests due to the enhanced light absorption for conversion efficiency improvement. To overcome the charge collection issue and the quantum dots degradation in the I^-/I_3^- electrolyte, we have investigated the addition of a nano-TiO_2 interfacial layer between CdS QDs and N719 dyes for enhancing the performance of the co-sensitized solar cell (**Fig. 20**). Atomic layer deposition is used to fabricate conformal and uniform TiO_2 interfacial layers with a thickness of 1.5 nm, 2.2 nm and 3.2 nm. It has been found that the addition of a TiO_2 interfacial layer can improve the device performance significantly (from 1.67% to 2.36%) through reducing the electron recombination and improving the QD stability in electrolyte, while there is an optimum thickness for the TiO_2 interfacial layer (**Figs. 21-24**)

We have demonstrated a novel and selective gas-sensing platform with reduced graphene oxide (RGO) decorated with tin oxide (SnO_2) nanocrystals (NCs) (**Fig. 25&26**). This hybrid SnO_2 NC-RGO platform showed enhanced NO_2 but weakened NH_3 sensing compared with bare RGO, showing promise in tuning the sensitivity and selectivity of RGO-based gas sensors (**Fig. 27**). We have also designed a new graphene-based hybrid nanostructure for anode materials in lithium-ion batteries (**Figs. 28&29**). The highly branched graphene nanosheets (HBGNs) directly grown on a copper current collector exhibited promising electrochemical performance due to their unique morphology, high electrical conductivity, large interfacial surface area, and high porosity (**Fig. 30**).

We have also developed a general and one-step approach to produce crumpled graphene (CG)-nanocrystal hybrids, which are produced by direct aerosolization of a GO suspension mixed with precursor ions (**Figs. 31&32**). Nanocrystals spontaneously grow from precursor ions and assemble on both external and internal surfaces of CG balls during the solvent evaporation and GO crumpling process. More importantly, CG-nanocrystal hybrids can be directly deposited onto various current-collecting substrates, enabling their tremendous potential for energy applications. As a proof of concept, we demonstrated the use of hybrid electrodes of CG-Mn_3O_4 and CG-SnO_2 in an electrochemical supercapacitor and a lithium-ion battery, respectively (**Figs. 33&34**). The performance of the resulting capacitor/battery was attractive and outperformed conventional flat graphene-based hybrid devices. This study provides a facile route to fabricating high-performance hybrid CG-nanocrystal electrodes for various energy systems.

Patents:

(1) J. H. Chen and Z. H. Wen, "Advanced Electrocatalysts for Oxygen Reduction Reaction," U.S. Provisional Patent Application 61/760,764 filed on Feb. 5, 2013.
(2) J. H. Chen, K. H. Yu, Z. Bo, and G. H. Lu, "High Electric Field Fabrication of Oriented Nanostructures," U.S. Provisional Patent Application (No. T130004US) filed in Sept. 2012.

Journal Publications:

(3) Z. Bo, K. H. Yu, G. H. Lu, S. Mao, and J. H. Chen*, "Understanding Growth of Carbon Nanowalls at Atmospheric Pressure Using Normal Glow Discharge Plasma-enhanced Chemical Vapor Deposition," *Carbon* **49**(6), 1849-1858, 2011. (IF=5.868)
(4) K. H. Yu, Z. Bo, G. H. Lu, S. Mao, S. M. Cui, Y. W. Zhu, X. Q. Chen, R. S. Ruoff, and J. H. Chen*, "Growth of Carbon Nanowalls at Atmospheric Pressure for One-step Gas Sensor Fabrication," *Nanoscale Research Letters* **6**:202, 2011. (IF=2.524)
(5) Z. Bo, K. H. Yu, G. H. Lu, S. M. Cui, S. Mao, and J. H. Chen*, "Vertically-oriented Graphene Sheets Grown on Metallic Wires for Greener Corona Discharges: Lower Power Consumption and Minimized Ozone Emission," *Energy & Environmental Science* **4**(7), 2525-2528, 2011. (IF=11.653)
(6) K. H. Yu, P. X. Wang, G. H. Lu, K. H. Chen, Z. Bo, and J. H. Chen*, "Patterning Vertically Oriented Graphene Sheets for Nanodevice Applications," *The Journal of Physical Chemistry Letters* **2**(6), 537-542, 2011. (IF=6.585)
(7) K. H. Yu, G. H. Lu, S. Mao, H. Kim, and J. H. Chen*, "Selective Deposition of CdSe Nanoparticles on Reduced Graphene Oxide to Understand Photoinduced Charge Transfer in Hybrid Nanostructures," *ACS Applied Materials & Interfaces* **3**(7), 2703-2709, 2011. (IF=5.008)
(8) S. Mao, K. H. Yu, S. M. Cui, Z. Bo, G. H. Lu, and J. H. Chen*, "A New Reducing Agent to Prepare Single-layer, High-quality Reduced Graphene Oxide for Device Applications," *Nanoscale* **3**(7), 2849-2853, 2011. (IF=6.233)
(9) K. H. Yu, G. H. Lu, Z. Bo, S. Mao, and J. H. Chen*, "Carbon Nanotube with Chemically-bonded Graphene Leaves for Electronic and Optoelectronic Applications," *The Journal of Physical Chemistry Letters* **2**(13), 1556-1562, 2011. (IF=6.585)
(10) Z. H. Wen, S. M. Cui, H. H. Pu, S. Mao, K. H. Yu, X. L. Feng*, and J. H. Chen*, "Metal Nitride/Graphene Nanohybrids: General Synthesis and Multifunctional Titanium Nitride/Graphene Electrocatalyst," *Advanced Materials* **23**(45), 5445-5450, 2011. (IF=14.829)
(11) Z. Bo, S. M. Cui, K. H. Yu, G. H. Lu, S. Mao, and J. H. Chen*, "Uniform Growth of Few-layer Graphene Vertically Standing on Cylindrical Surface at Atmospheric Pressure," *Review of Scientific Instruments* **82**(8), 086116, 2011. (IF=1.602)
(12) Z. H. Wen, S. Q. Ci, F. Zhang, X. L. Feng, S. M. Cui, S. Mao, S. L. Luo, and Z. He*, and J. H. Chen*, "Nitrogen-Enriched Core-Shell Structured Fe/Fe3C-C Nanorods as Advanced Catalysts for Oxygen Reduction Reaction," *Advanced Materials* **24**(11), 1399-1404, 2012. **(Featured as Frontispiece)** (IF=14.829)
(13) Z. H. Wen, S. M. Cui, H. J. Kim, S. Mao, K. H. Yu, G. H. Lu, H. H. Pu, O. Mao, and J. H. Chen*, "Binding Sn-Based Nanoparticles on Graphene as Anode of

Lithium Ions Batteries," *Journal of Materials Chemistry* **22**(8), 3300-3306, 2012. (IF=6.101)

(14) K. H. Yu, G. H. Lu, K. H. Chen, S. Mao, H. Kim, and J. H. Chen*, "Controllable Photoelectron Transfer in CdSe Nanocrystal-Carbon Nanotube Hybrid Structures," *Nanoscale* **4**(3), 742-746, 2012. (IF=6.233)

(15) S. Mao, H. H. Pu, and J. H. Chen*, "Graphene Oxide and Its Reduction: Modeling and Experimental Progress," *RSC Advances* **2**(7), 2643-2662, 2012. **(Top 10 accessed article in March, April, and May 2012)** (IF=2.562)

(16) H. J. Kim, Z. H. Wen, K. H. Yu, O. Mao, and J. H. Chen*, "Straightforward Fabrication of Highly Branched Graphene Nanosheet Array for Li-ion Battery Anode," *Journal of Materials Chemistry* **22**(31), 15514-15518, 2012. (IF=6.101)

(17) Z. Bo, S. Mao, K. H. Yu, S. M. Cui, and J. H. Chen*, "One-step Fabrication and Capacitive Behavior of Electrochemical Double Layer Capacitor Electrodes Using Vertically-oriented Graphene Directly Grown on Metal," *Carbon* **50**(12), 4379-4387, 2012. (IF=5.378)

(18) S. Mao, S. M. Cui, G. H. Lu, K. H. Yu, Z. H. Wen, and J. H. Chen*, "Tuning Gas-sensing Properties of Reduced Graphene Oxide Using Tin Oxide Nanocrystals," *Journal of Materials Chemistry* **22**(22), 11009-11013, 2012. (IF=6.101)

(19) K. H. Yu, X. Lin, G. H. Lu, Z. H. Wen, C. Yuan*, and J. H. Chen*, "Optimizing CdS Quantum Dot Sensitized Solar Cell Performance through Atomic Layer Deposition of Ultrathin TiO_2 Coating," *RSC Advances* **2**(20), 7843-7848, 2012. (IF=2.562)

(20) Z. H. Wen, X. C. Wang, S. Mao, Z. Bo, H. Kim, S. M. Cui, G. H. Lu, X. L. Feng*, and J. H. Chen*, "Crumpled Nitrogen-Doped Graphene Nanosheets with Ultrahigh Pore Volume for High-performance Supercapacitor," *Advanced Materials* **24**(41), 5610-5616, 2012. (IF=14.829)

(21) X. Lin, K. H. Yu, G. H. Lu, J. H. Chen*, and C. Yuan*, "Improving Conversion Efficiency of Quantum Dot and Dye Co-Sensitized Solar Cells through Atomic Layer Deposition of TiO_2 Interfacial Layer," *Journal of Physics D: Applied Physics* **46**(2), 024004, 2013. (IF=2.528) (**Invited Paper**)

(22) S. M. Cui, S. Mao, G. H. Lu, and J. H. Chen*, "Graphene Coupled with Nanocrystals: Opportunities and Challenges for Energy and Sensing Applications," *The Journal of Physical Chemistry Letters* **2**(13), 1556-1562, 2013. (**Invited Perspective**, IF=6.585)

(23) X. F. Gao, J. H. Chen, and C. Yuan*, "Free-Standing TiO_2 Nanotube Arrays with Ultraprecise Control of Wall Thickness for Dye-Sensitized Solar Cells," *Journal of Power Sources* **240**, 503-509, 2013. (IF=4.675)

(24) S. Mao, K. H. Yu, J. B. Chang, D. A. Steeber, L. Ocola, and J. H. Chen*, "Direct Growth of Vertically-aligned Graphene for Field-Effect Transistor Biosensor," *Scientific Reports* **3**, No. 1696, 2013. (IF=2.927)

(25) Z. Bo*, Y. Yang, K. H. Yu, J. H. Chen, J. H. Yan, and K. F. Cen, "Plasma-Enhanced Chemical Vapor Deposition Synthesis of Vertically-oriented Graphene Nanosheets: A Review," *Nanoscale* **5**(12), 5180-5204, 2013. (IF=6.233)

(26) S. Mao, Z. H. Wen, H. J. Kim, G. H. Lu, P. T. Hurley, and J. H. Chen*, "A General Approach to One-Pot Fabrication of Crumpled Graphene-Based Nanohybrids for Energy Applications," *ACS Nano* **6**(8), 7505-7513, 2012. (IF=12.062)

(27) G. H. Lu, K. H. Yu, Z. H. Wen, and J. H. Chen*, "Semiconducting Graphene: Converting Graphene from Semimetal to Semiconductor," *Nanoscale* **5**(4), 1353-1368, 2013. (**Invited Review**, IF=6.233)

(28) Y. Hou, Z. H. Wen, S. M. Cui, X. R. Guo, and J. H. Chen*, "Constructing 2D Porous Graphitic C_3N_4 Nanosheets/Nitrogen-Doped Graphene/Layered MoS_2 Ternary Nanojunction with Enhanced Photoelectrochemical Activity," *Advanced Materials* **25**(43), 6291-6297, 2013*.* **(VIP paper)** (IF=14.829)

(29) X. F. Gao, D. S. Guan, J. W. Huo, J. H. Chen, and C. Yuan*, "Free Standing TiO_2 Nanotube Array Electrodes with Ultra-Thin Al_2O_3 Barrier Layer and $TiCl_4$ Surface Modification for High Efficiency Dye Sensitized Solar Cells," *Nanoscale* **5**(21), 10438-10446, 2013*.* (IF=6.233)

Invited Presentations:

(30) **Invited Presentation**: "Hybrid Nanomaterials for Chemical and Biological Sensing," **University of Wisconsin-Stevens Point**, Department of Chemistry, Stevens Point, WI, April 2011.

(31) **Invited Presentation**: "Advanced Nanomaterials for Sensing Applications," **A. O. Smith Corporation**, Milwaukee, WI, April 2011.

(32) **Invited Presentation**: "Hybrid Nanomaterials for Sensing Applications," **ASM International Milwaukee Chapter 53rd Annual H. R. Bergmann Memorial Seminar**, Milwaukee, WI, May 2011.

(33) **Invited Presentation**: "Hybrid Nanomaterials for Chemical and Biological Sensing," **University of Georgia**, Department of Physics, Athens, GA, January 2011.

Conference Presentations:

(34) K. H. Yu, H. Kim, G. H. Lu, and J. H. Chen, "Optoelectronic Properties of Hybrid Nanostructures of CdSe Nanoparticles Supported on Graphene," Presented at the *2010 ASME IMECE*, Vancouver, British Columbia, CA, November 12-18, 2010.

(35) K. H. Yu, H. Kim, G. H. Lu, and J. H. Chen, "CdSe Nanoparticles on Graphene for Photovoltaic Applications," Presented at *the 29th AAAR Conference*, Portland, OR, October 25-29, 2010.

(36) K. H. Yu, G. H. Lu, S. Mao, K. H. Chen, H. Kim, Z. H. Wen, and J. H. Chen, "Selective Deposition of CdSe Nanoparticles on Reduced Graphene Oxide to Understand Photoinduced Charge Transfer in Hybrid Nanostructures**,**" *Abstracts of the MRS Fall Meeting,* Boston, MA, November 28-December 2, 2011.

(37) K. H. Yu, P. X. Wang, G. H. Lu, K. H. Chen, Z. Bo, and J. H. Chen, "Patterning Vertically Oriented Graphene Sheets for Nanodevice Applications**,**" *Abstracts of the MRS Fall Meeting,* Boston, MA, November 28-December 2, 2011.

(38) S. Mao, K. H. Yu, S. M. Cui, Z. Bo, G. H. Lu, and J. H. Chen, "A New Reducing Agent to Prepare Single-Layer, High-Quality Reduced Graphene Oxide for Device Applications**,"** *Abstracts of the MRS Fall Meeting,* Boston, MA, November 28-December 2, 2011.

(39) K. H. Yu, G. H. Lu, Z. Bo, S. Mao, and J. H. Chen, "Carbon Nanotube with Chemically Bonded Graphene Leaves for Electronic and Optoelectronic

Applications**,**" *Abstracts of the MRS Fall Meeting,* Boston, MA, November 28-December 2, 2011.

(40) H. Kim, Z. H. Wen, K. H. Yu, G. H. Lu, O. Mao, and J. H. Chen, "Nanocarbon Decorated with Sn Nanoparticles for Lithium-ion Batteries," *Abstracts of the 2011 ASME IMECE*, Denver, CO, November 11-17, 2011.

(41) K. H. Yu, G. H. Lu, Z H. wen, H. Kim, Y. Y. Qian, E. Andrew, S. Mao, and J. H. Chen, "Functionalized Vertical Graphene as a Catalytic Counter Electrode in Dye-Sensitized Solar Cells," Presented at the *2012 ASME IMECE*, Houston, TX, November 9-15, 2012.

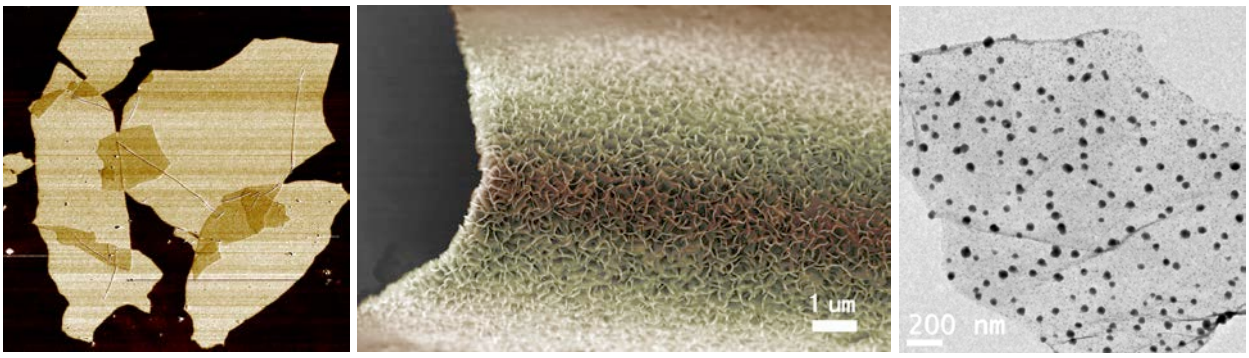

Fig. 1. (a) Atomic force microscopy (AFM) image of as-produced GO sheets. (b) Carbon nanowalls produced by PECVD. (c) CdSe nanoaprticle-coated graphene sheet.

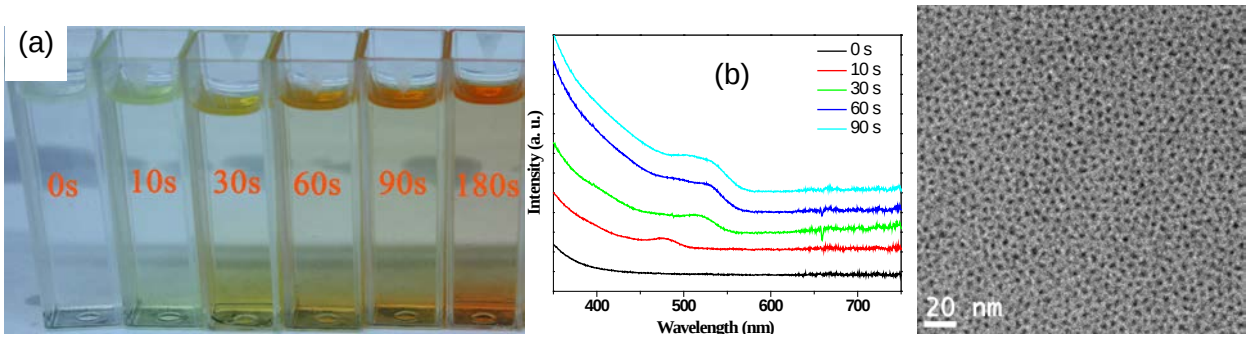

Fig. 2. CdSe QDs synthesized in Chen's Laboratory: (a) digital photo; (b) UV-VIS absorption spectra; and (c) TEM image.

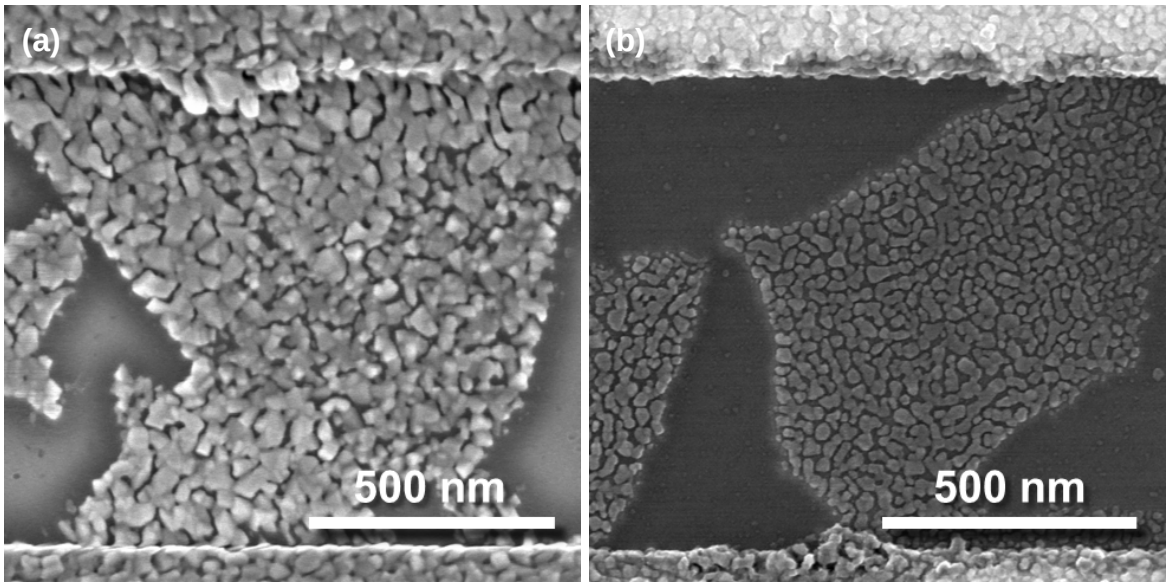

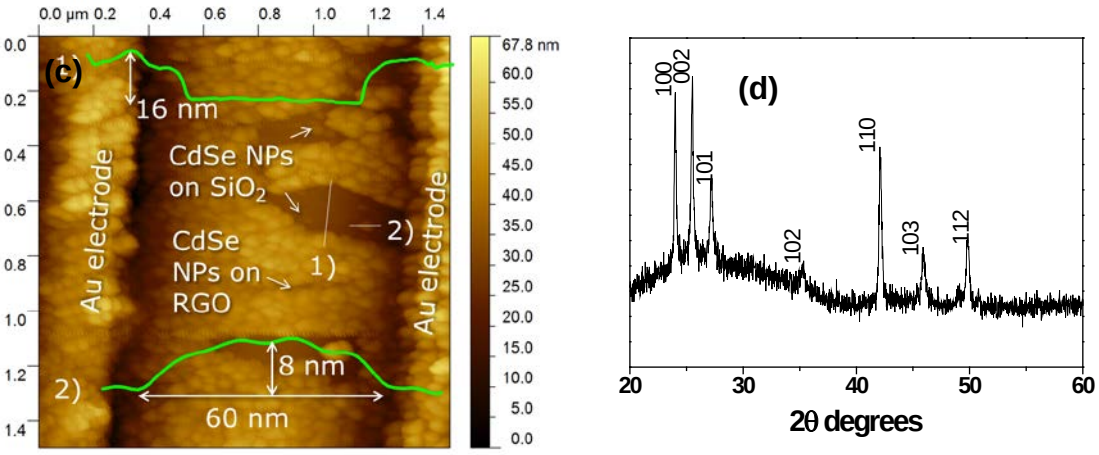

Fig. 3. SEM images of (a) a G-*h*NP photodetector, (b) a G-*l*NP photodetector. (c) AFM images of a G-*h*NP photodetector. The insets in (c) are the height profiles taken along white lines labeled as 1) and 2). (d) XRD 2θ scan of the CdSe NPs.

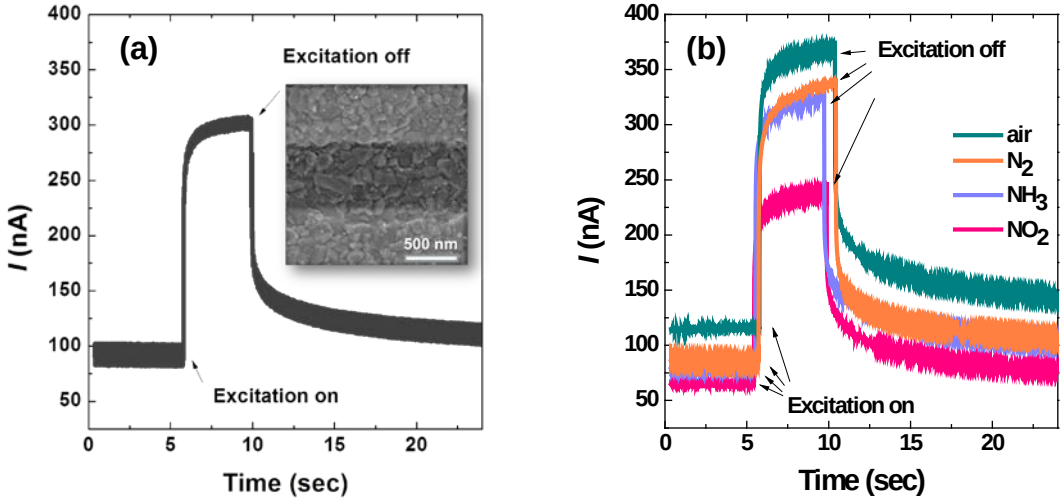

Fig. 4. Photoinduced current response versus time of a G-*h*NP photodetector under irradiation of (a) simulated sunlight 100 mW cm^{-2} (AM 1.5 G) in air, and (b) 532-nm laser of ~ 50 mW with different gas flows of air, N_2, NH_3, and NO_2. Inset of (a) is an SEM image of the corresponding device. All current changes were recorded with a bias voltage of 0.01 V.

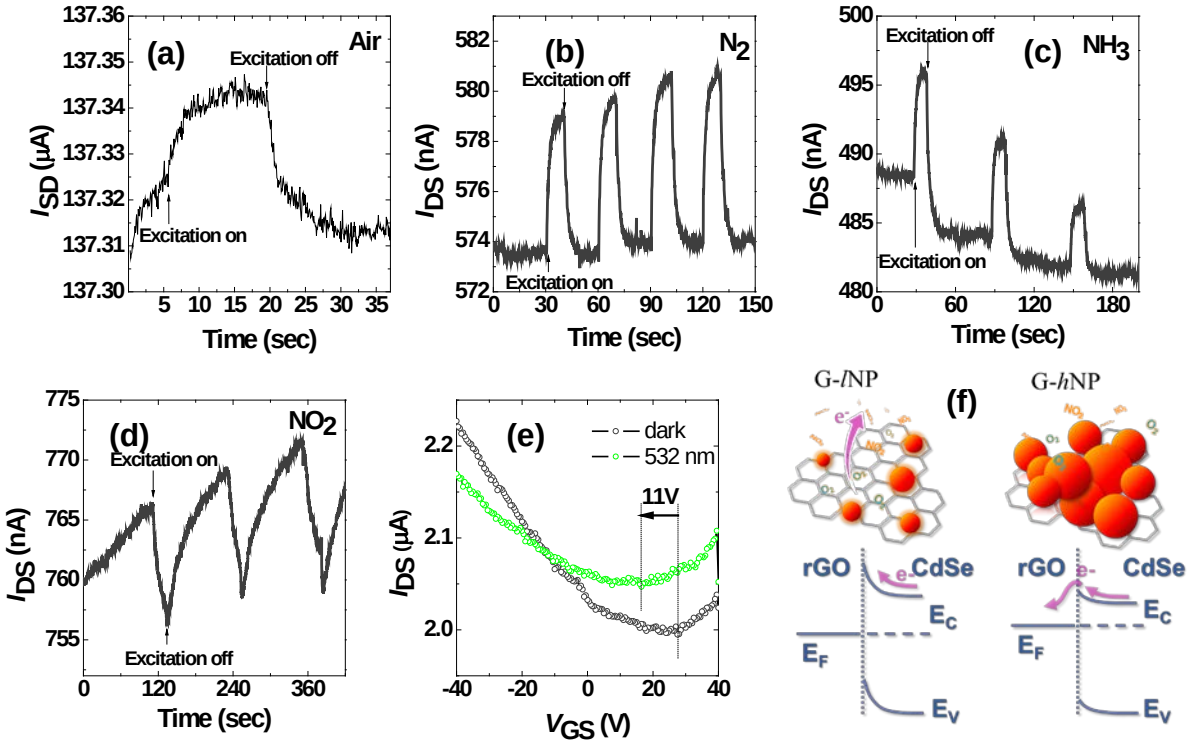

Fig. 5. Photoinduced current response versus time of a G-*l*NP photodetector under chopped irradiation of a 532-nm laser of ~ 50 mW in different gases (a) air, (b) N_2, (c) NH_3, and (d) NO_2. All current changes were recorded under a bias voltage of 0.01 V. (e) Drain-source current versus back gate voltage of a PMMA-coated G-*l*NP photodetector with and without laser irradiation. The drain-source bias voltage was 0.1 V. (f) Energy band bending caused by gases at the interface between CdSe NPs and R-GO of G-*l*NP and G-*h*NP photodetectors.

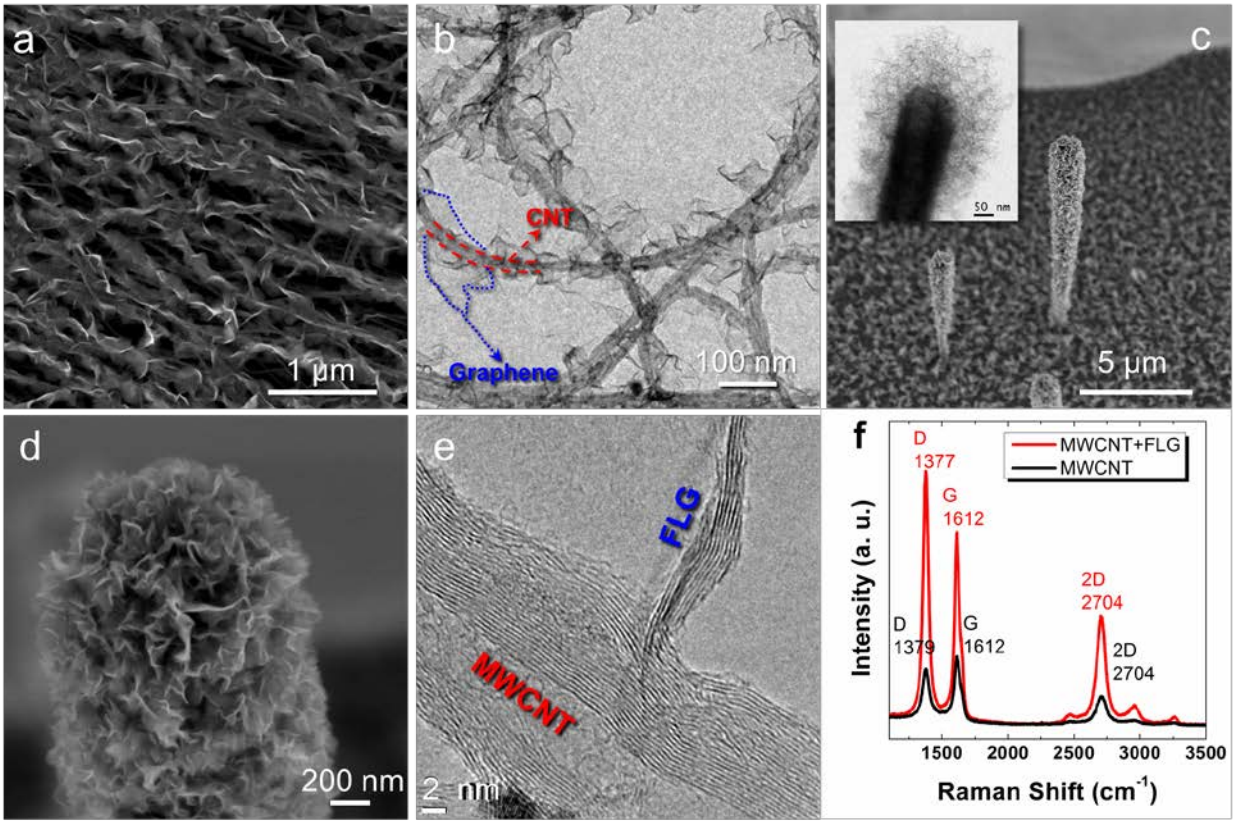

Fig. 6. (a) SEM image of CNT-FLG hybrid structures. (b) TEM image of FLGs grown on CNTs suspended on a Cu TEM grid. (c) SEM image of FLGs grown on vertically-aligned CNTs; the inset is a TEM image of the tip of a CNT-FLG, where the CNT stem (dark) is clearly distinguished from FLGs (bright). (d) A close view of the CNT-FLG tip in (c). (e) HRTEM image of a CNT-FLG structure showing that the FLG is inherently bonded to the host CNT. (f) Raman spectra of pristine CNT (black) and CNT-FLG (red) films.

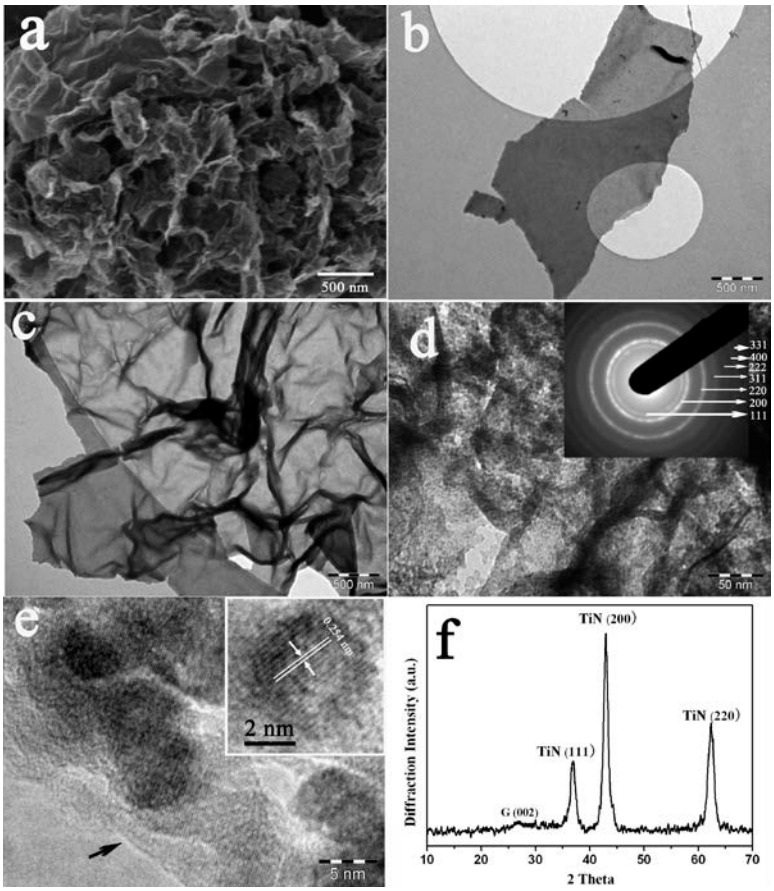

Fig. 7. SEM image (a), TEM images (b-d), HRTEM image (e), and XRD pattern (f) of the TiN/NG nanohybrids; inset of (d) is the corresponding SAED pattern and inset of (e) is a typical TiN nanoparticle on the NG surface.

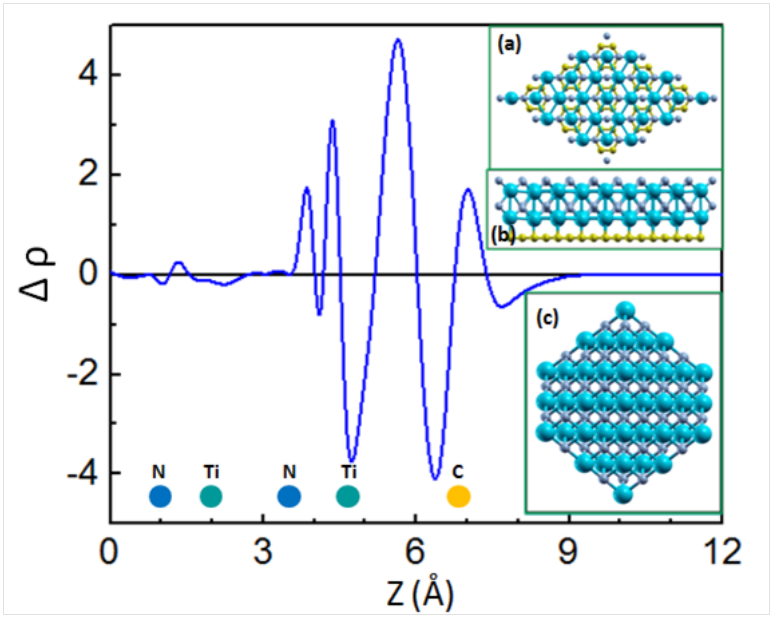

Fig. 8. Plane-averaged charge density difference along the vertical direction showing the electron redistribution upon formation of the graphene-TiN(111) interface at the Ti

surface. Colored spheres indicate the positions of atom layers. Inset: (a) projected view of graphene and TiN (111) complex system; (b) and (c) are views along the (111) face for graphene-TiN (111) complex system and bulk TiN crystal.

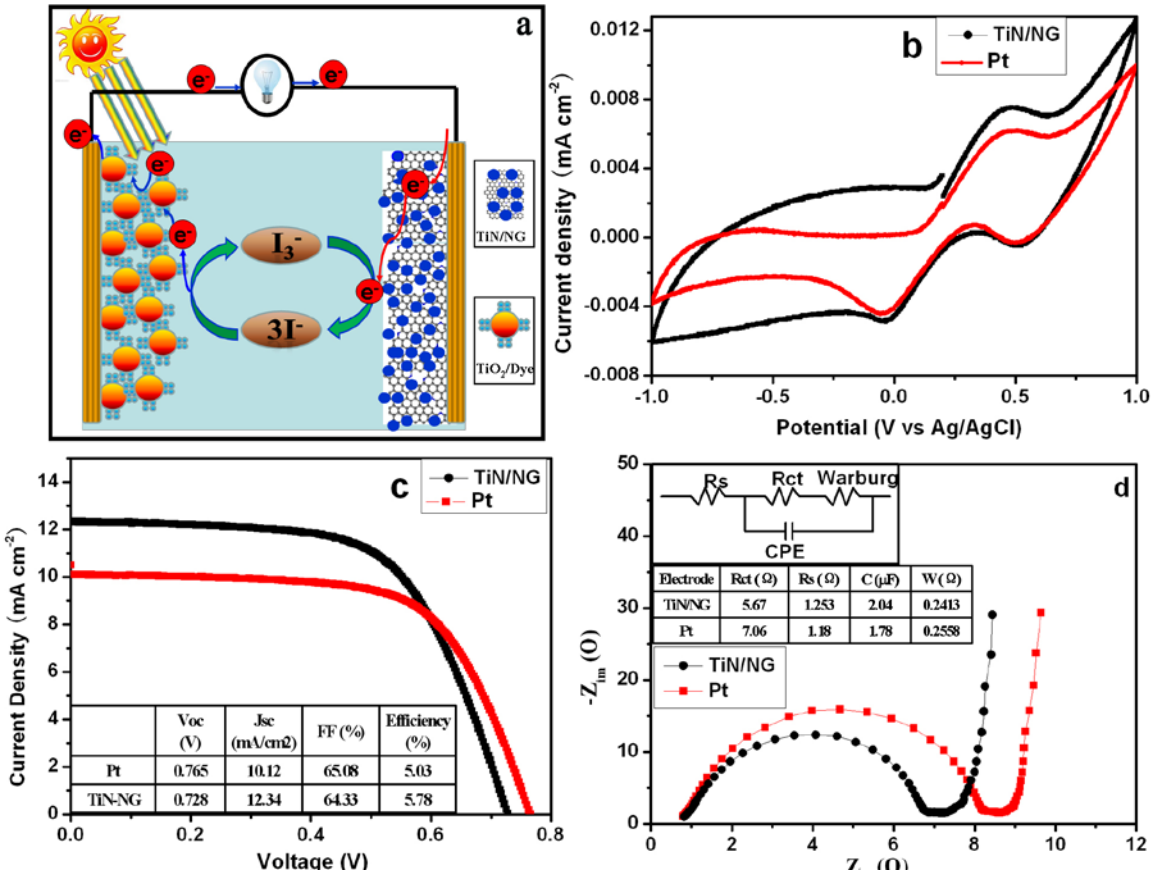

Fig. 9. (a) Schematic illustration of a DSSC using TiN/NG as the counter electrode; (b) Cyclic voltammogram for TiN/NG and Pt counter electrodes in 1.0 mM LiI and 0.1 mM I_2 acetonitrile solution containing 0.1 M $LiClO_4$ as the supporting electrolyte; reference electrode: Ag/AgCl; counter electrode: platinum wire. (c) Characteristic J–V curves of DSSCs with TiN/NG and Pt counter electrodes measured under simulated sunlight 100 mW cm^{-2} (AM 1.5); inset table: photovoltaic parameters of DSSCs with different counter electrodes. (d) Equivalent circuit, EIS parameters and Nyquist plots of the TiN/NG and Pt modified ITO-electrode in 1.0 mM LiI and 0.1 mM I2 acetonitrile solution containing 0.1 M $LiClO_4$ over the frequency range 100 kHz~5 mHz; R_{ct} : Charge-transfer resistance; W: Warburg impedance; R_s: Ohmic internal resistance; C: constant phase element.

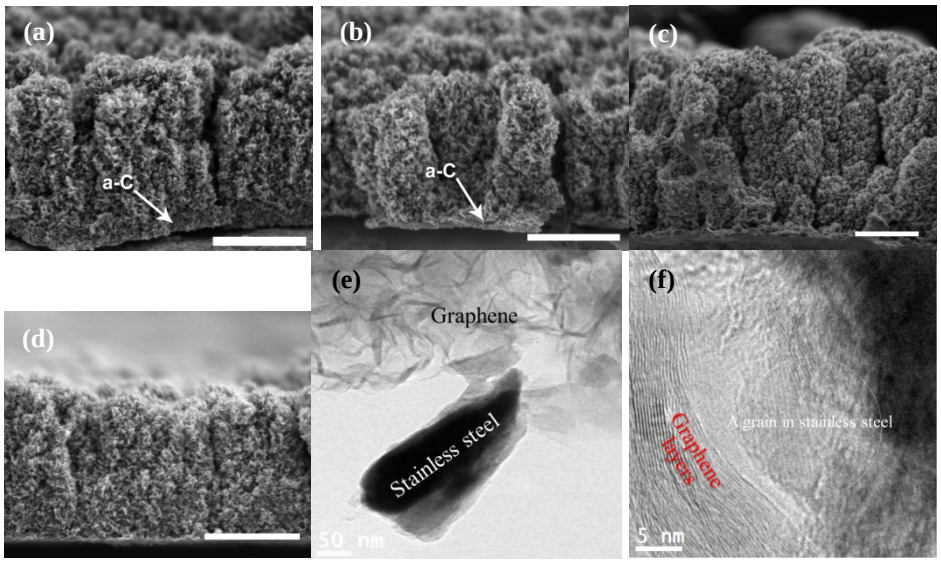

Fig. 10. Electron microscopy characterization of VG grown on a stainless steel plate. (a-d) SEM image of the cross-sectional view of the VG electrodes: (a) VG-1, (b) VG-2, (c) VG-3, (d) VG-4. The scale bar in SEM images is 1 μm. Amorphous carbon (a-C) can be seen at bottom of the VG film of (a) and (b). (e) TEM image of graphene sheets grown off a stainless steel substrate. (f) Graphene layers and stainless steel grain can be identified in the HRTEM image.

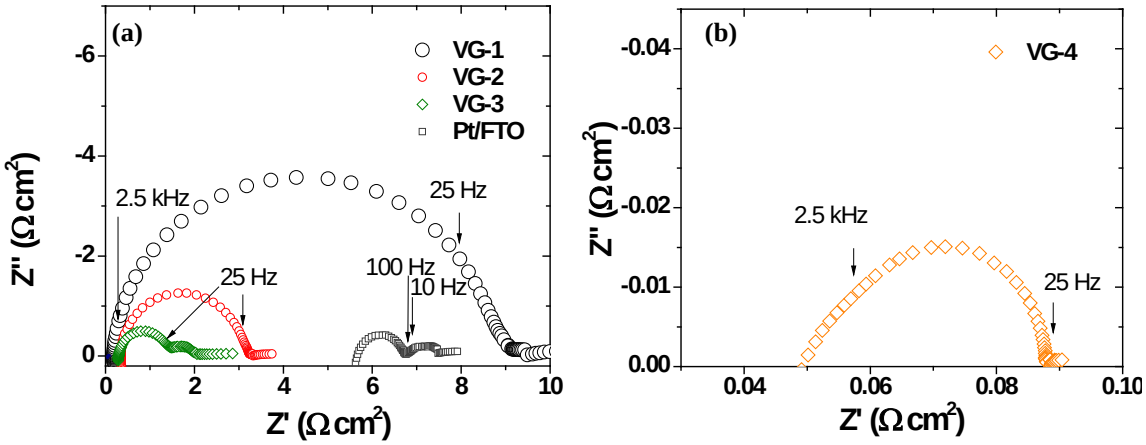

Fig. 11. Nyquist plots of electrochemical impedance spectra measured from 100 kHz to 0.1 Hz on symmetrical dummy cells with (a) VG-1, VG-2, VG-3, Pt/FTO, and (b) VG-4 (bias 0 V).

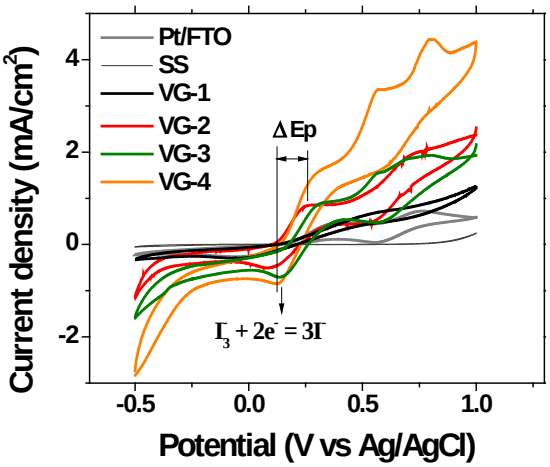

Fig. 12. Cyclic voltammograms obtained at a scan rate of 20 mV/s for the oxidation and reduction of I_2/I_3^- and I^-/I_3^- redox couples using the as-grown VG on stainless steel plates as working electrodes. A Pt/FTO electrode was measured for comparison. A blank stainless steel (SS) electrode was also scanned for the background signal. The peak-to-peak separation (ΔE_p) and reduction of I_3^- are indicated.

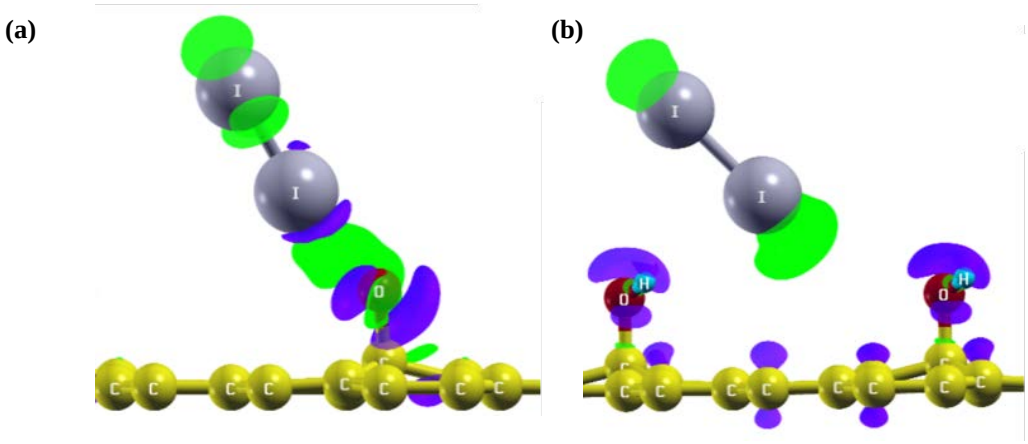

Fig. 13. Side views of contour plots of charge transfer between molecular I_2 and graphene oxidized with functional groups, (a) epoxy with charge transfer constant 0.00250 e and (b) hydroxyl with charge transfer constant 0.00125 e. The green and the purple color represent charge accumulation and depletion zone, respectively.

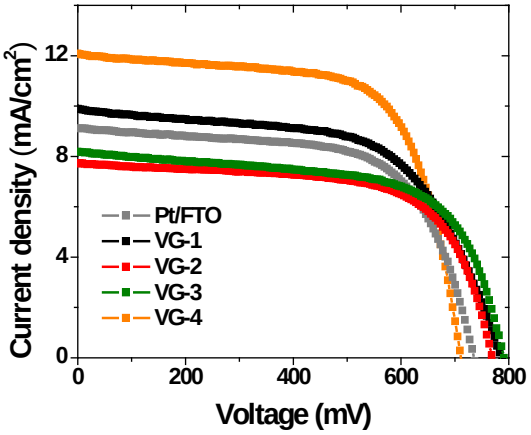

Fig. 14. Current density-voltage characteristics of DSSCs with platinized FTO and VG counter electrodes. The illumination intensity is one sun, AM 1.5G, 100 mW/cm^2.

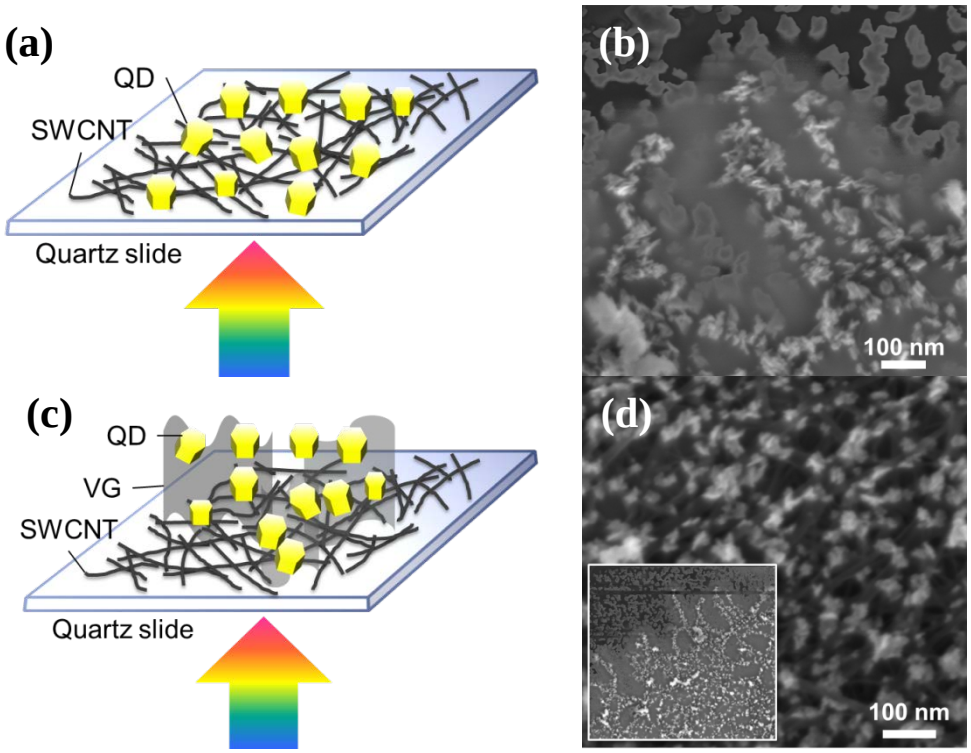

Fig. 15. Schematic configurations of (a) QD-CNT and (c) QD-VG-CNT photoanodes. SEM images of (b) SWCNT and (d) VG-SWCNT decorated with CdS QDs. The inset of (b) is an overview of the QD-VG-SWCNT network.

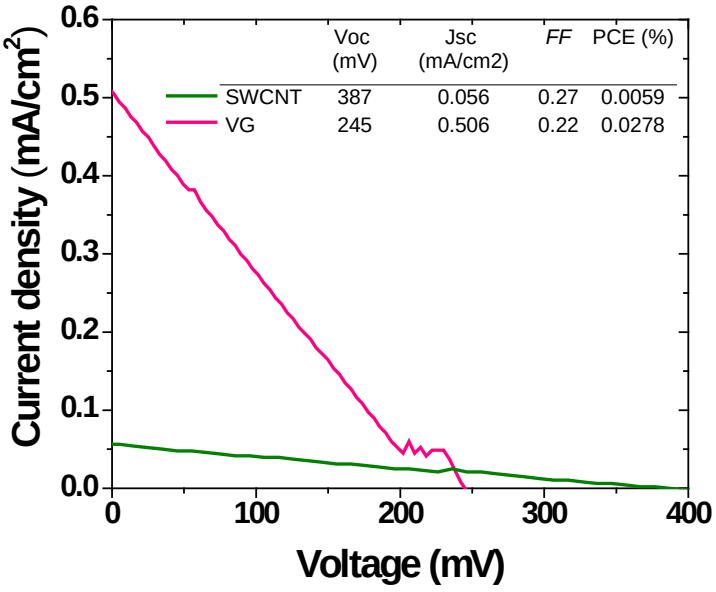

Fig. 16. I-V characteristics of QD-VG-CNT (red) and QD-CNT (green) cells under illumination of one sun (AM 1.5G, 100 mW/cm^2). The inset table is a summary of cell parameters.

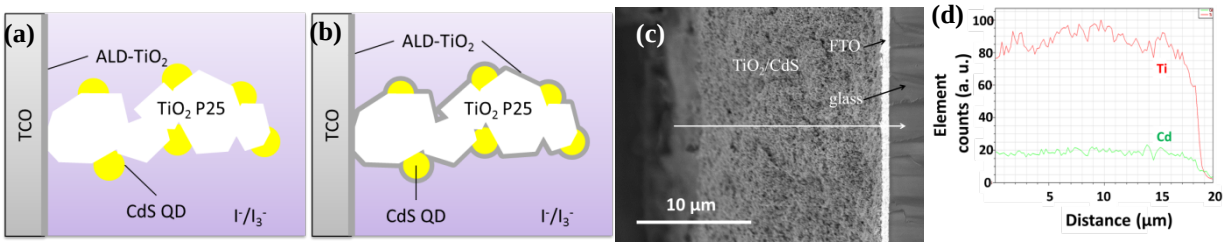

Fig. 17. Schematics of the CdS QD-sensitized nanocrystalline TiO_2 electrode (a) without and (b) with ALD-TiO_2 protection layer. (c) Cross-sectional SEM image of the CdS QD-sensitized mesoporous TiO_2 film with 100c ALD-TiO_2 coating supported on FTO glass. (d) EDS analysis of Ti and Cd along the white arrow in (c).

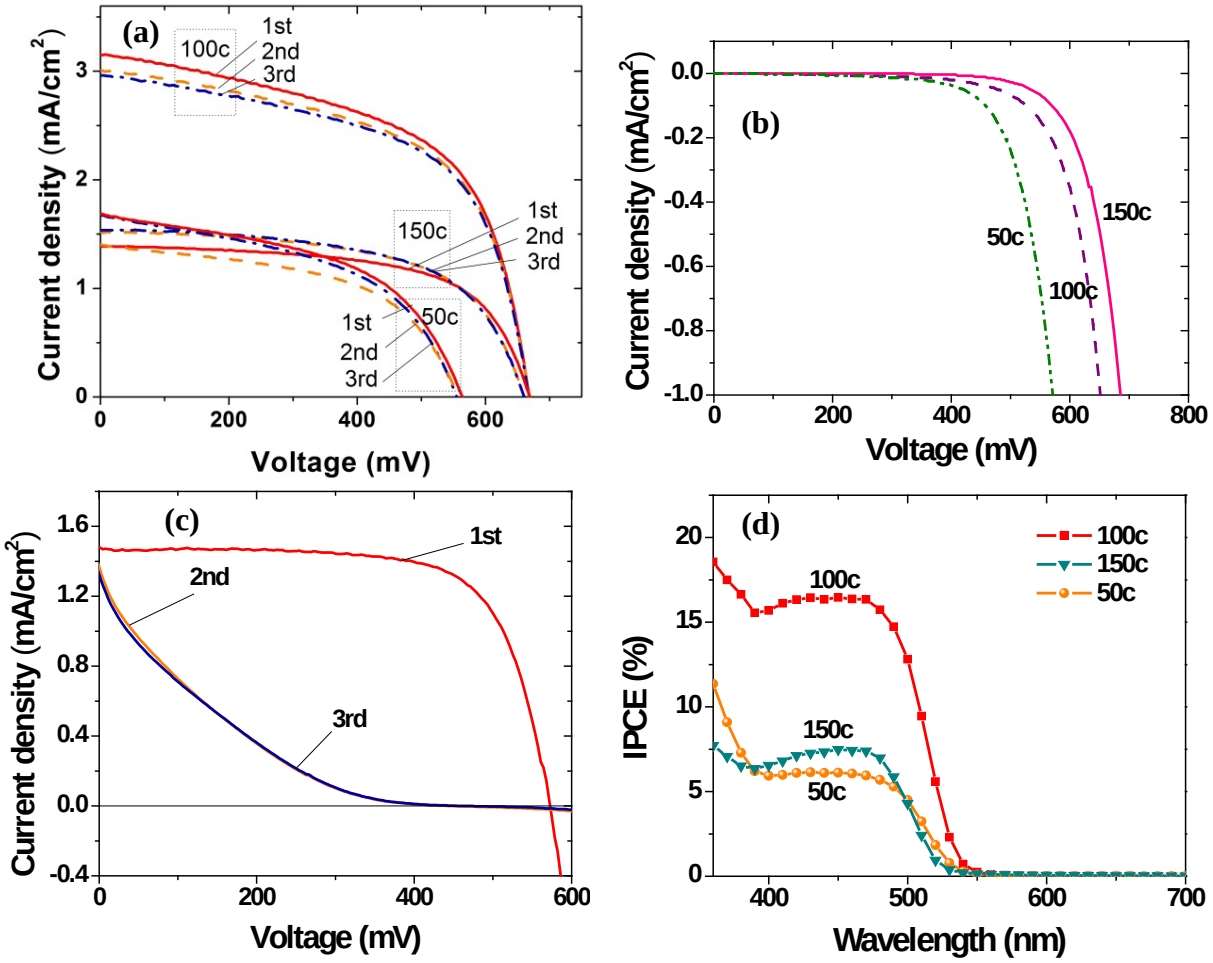

Fig. 18. Characterization of the CdS-QDs sensitized TiO_2 solar cells with and without ALD-TiO_2 protection layer. I-V measurements of three differently coated cells (50c, 100c, and 150c) (a) under illumination of one sun (AM 1.5G, 100 mW/cm^2) and (b) under dark conditions. For the curves measured under illumination, each cell was measured three times: solid line (first time), dashed line (second time), and dash-dotted line (third time). (c) I-V measurement of a non-coated cell under illumination of one sun (AM 1.5G, 100 mW/cm^2) for three times. (d) IPCE of the three differently coated cells.

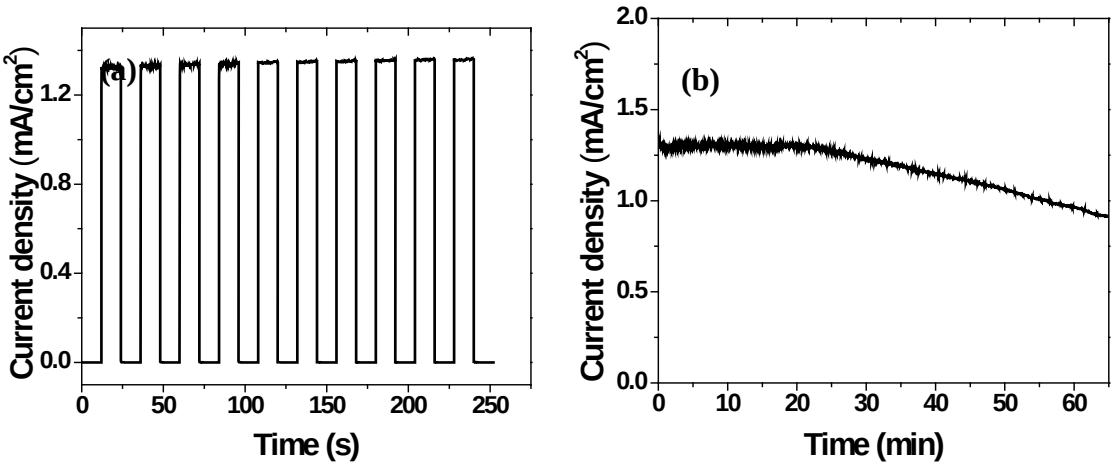

Fig. 19. Photo-stability test of a 100c solar cell. (a) Short circuit current density as a function of time using periodic illumination intervals (12 s interval length). (b) Short circuit current versus time of a 100c solar cell under illumination of one sun (AM 1.5G, 100 mW/cm^2) over 1 hour.

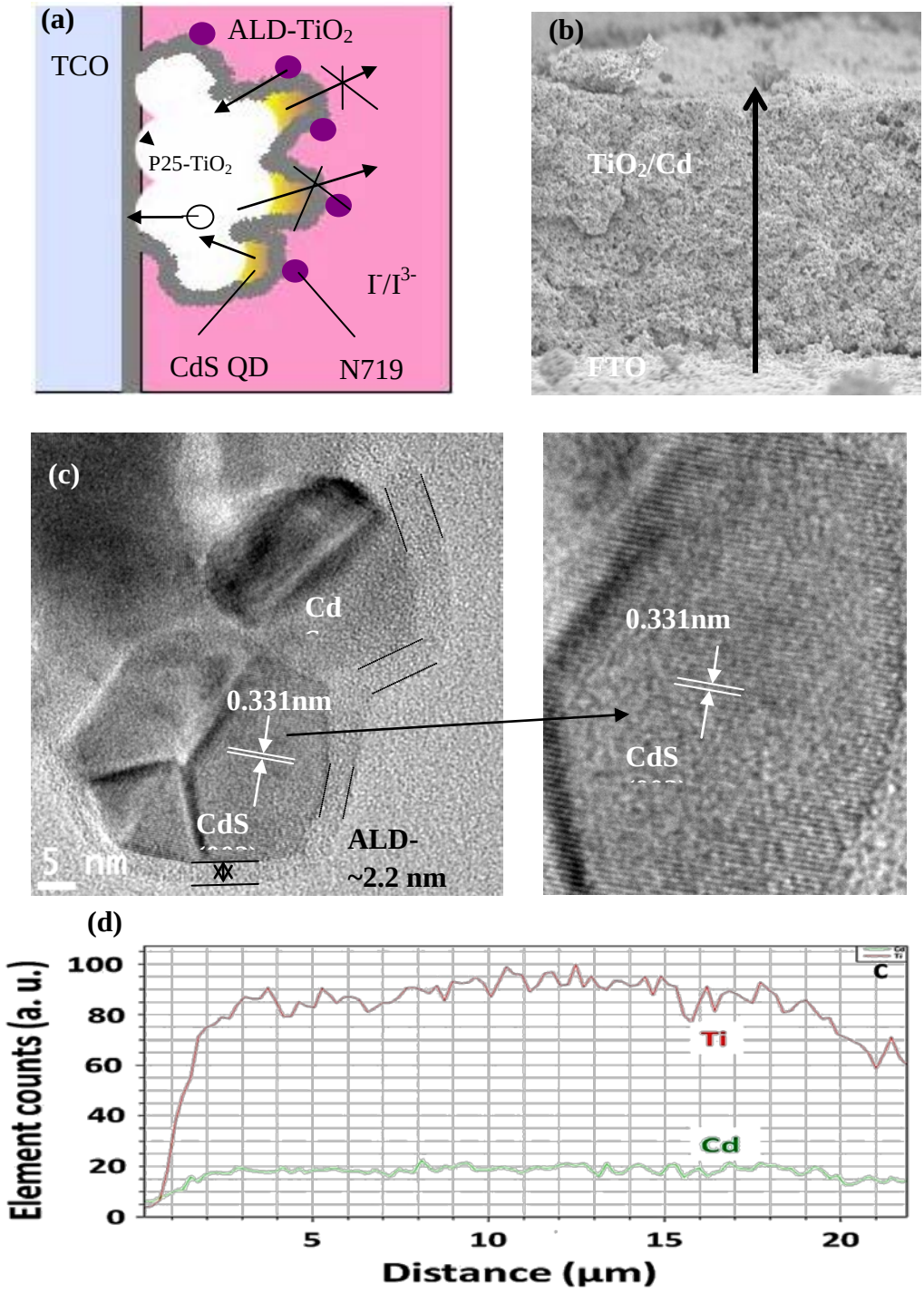

Fig. 20. (a). schematic of the CdS/N719 co-sensitized solar cell; b). cross sectional SEM image of the CdS/N719 co-sensitized mesoporous TiO_2 anode; (c). HRTEM image of CdS quantum dot coated by TiO_2; (d) EDS line-scan analysis along the arrow in (a) of the CdS/N719 co-sensitized solar cell electrode.

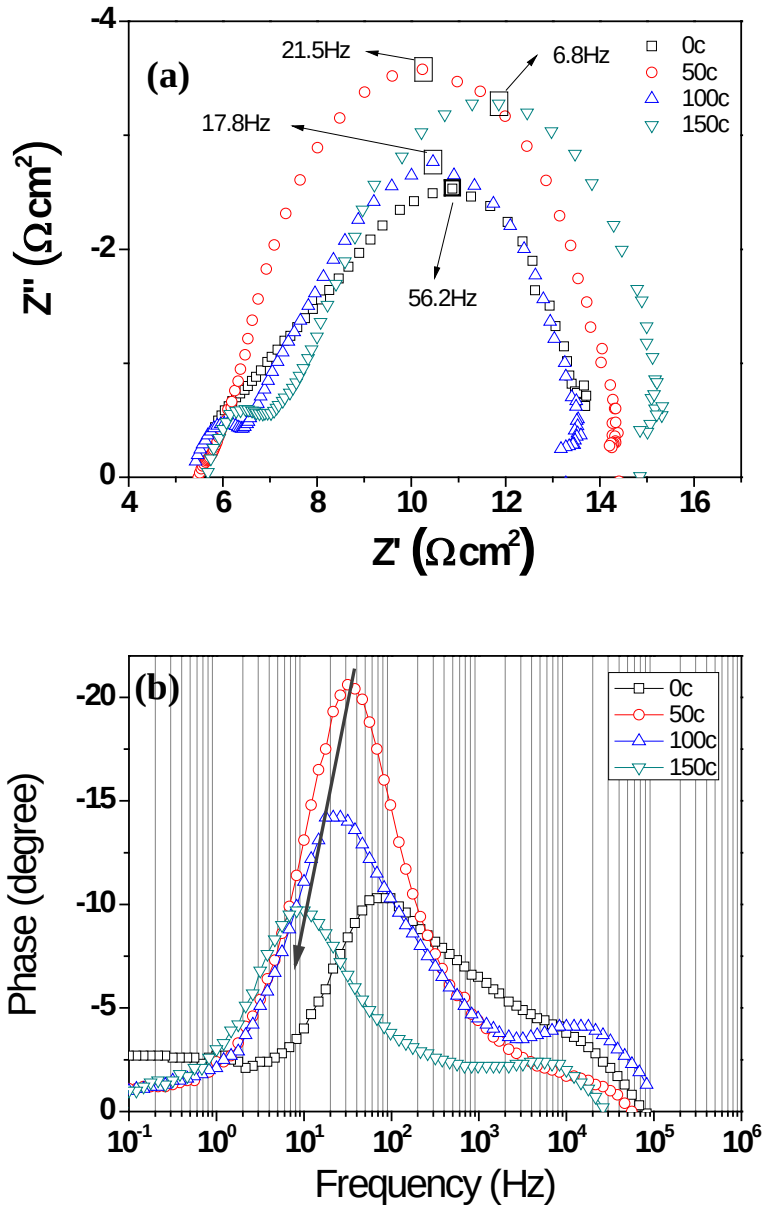

Fig. 21. EIS results of the CdS QD and N719 dye co-sensitized solar cells with/without TiO_2 interfacial layers (a) EIS Nyquist plots and (b) Bode phase plots.

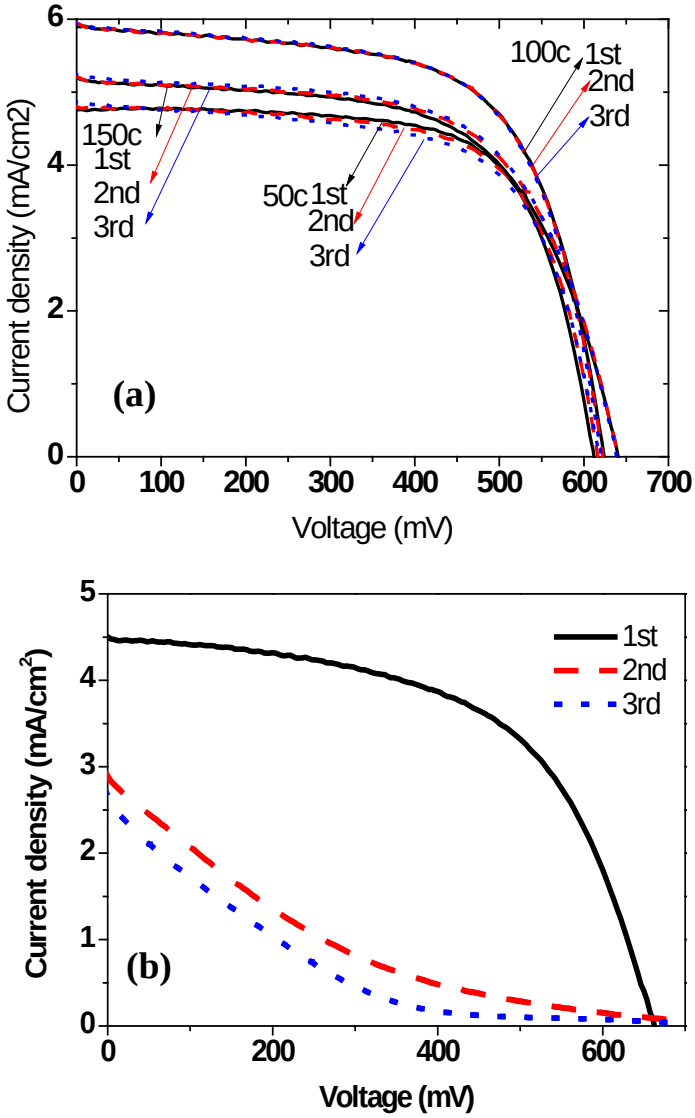

Fig. 22. a). I-V characteristics of the CdS QD and N719 dye co-sensitized solar cells with different ALD coated TiO_2 interfacial layers; b). I-V degradation of the CdS QD and N719 dye co-sensitized solar cell without TiO_2 interfacial layers.

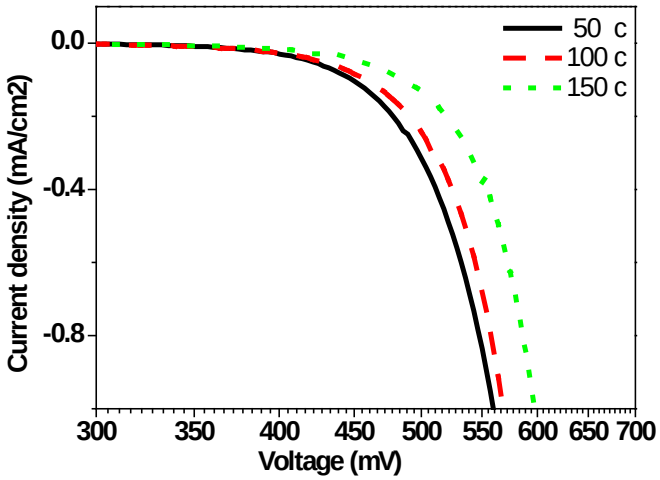

Fig. 23. I-V measurements (dark) of the CdS QD and N719 Dye co-sensitized solar cells with TiO_2 interfacial layers.

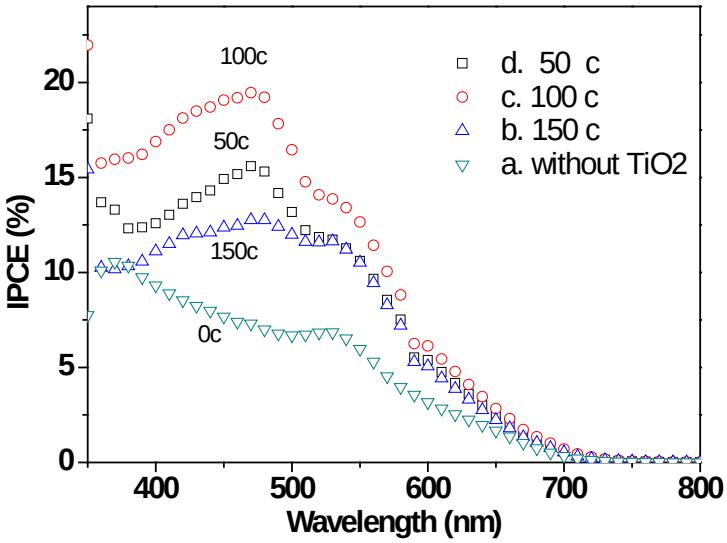

Fig. 24. IPCE of the QD and dye co-sensitized solar cells.

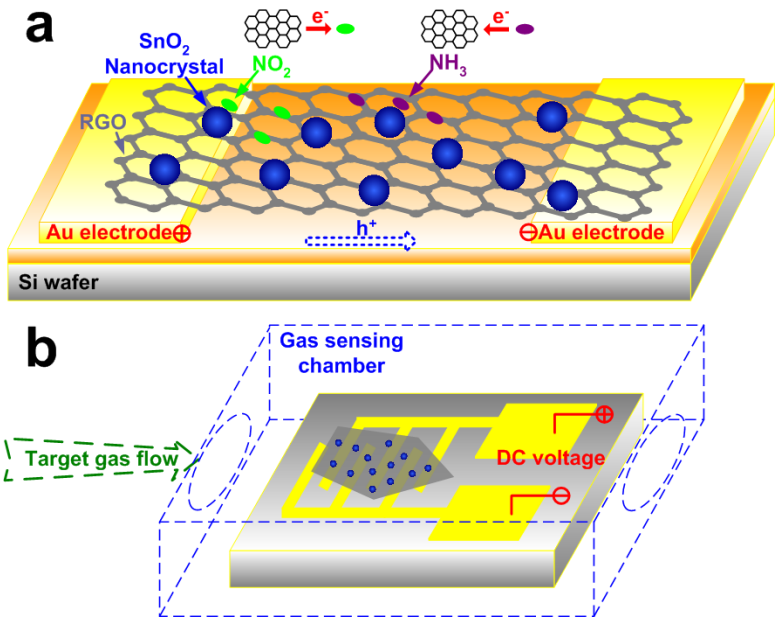

Fig. 25. (a) Schematic of the novel gas-sensing platform of an RGO sheet decorated with SnO_2 NCs. (b) Schematic of the sensor testing system.

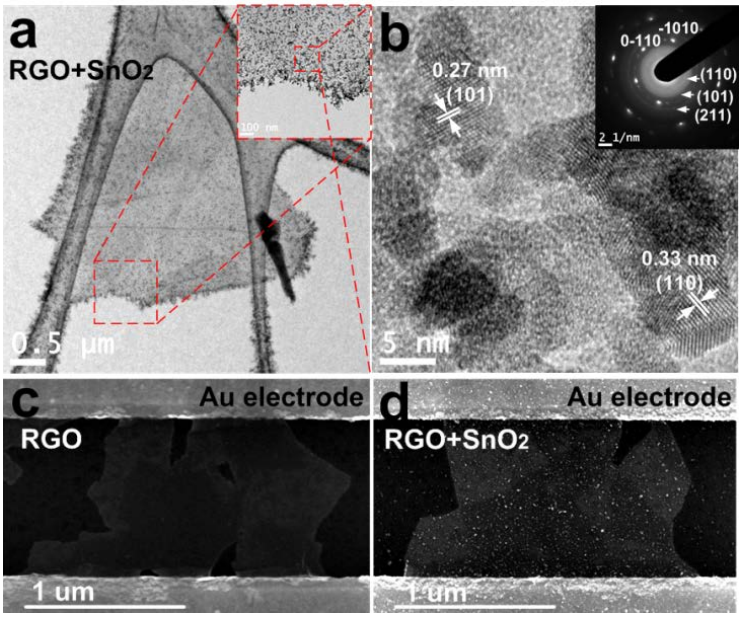

Fig. 26. (a) TEM and (b) HRTEM images of the RGO sheet decorated with SnO_2 NCs. The inset shows the SAD patterns of the RGO sheet and SnO_2 NCs. (c) SEM image of RGO sheets bridging a pair of Au electrode fingers. (d) SEM image of the RGO sheets decorated with SnO_2 NCs bridging a pair of Au electrode fingers.

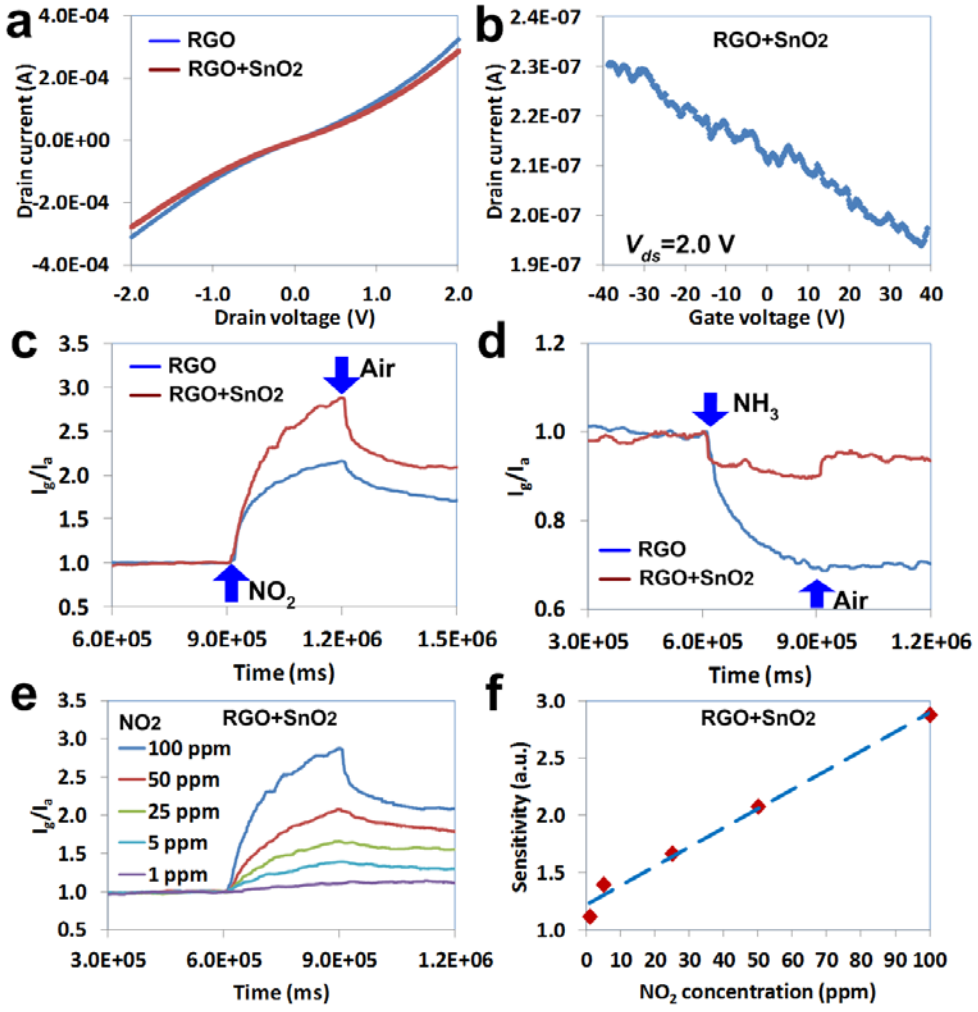

Fig. 27. (a) Direct current measurement results of RGO before and after SnO_2 NC decoration. (b) FET measurement result (V_{ds} = 2.0 V) of the SnO_2 NC-RGO sensor. (c) and (d), gas sensing signals of NO_2 and NH_3 from RGO sensors with and without SnO_2 NCs. The sensing signal is normalized by the measured sensor current in air (base line, I_g/I_a=1). (e) SnO_2 NC-RGO sensor response to NO_2 at various concentrations. (f) The sensitivity of the SnO_2 NC-RGO sensor vs. NO_2 concentration.

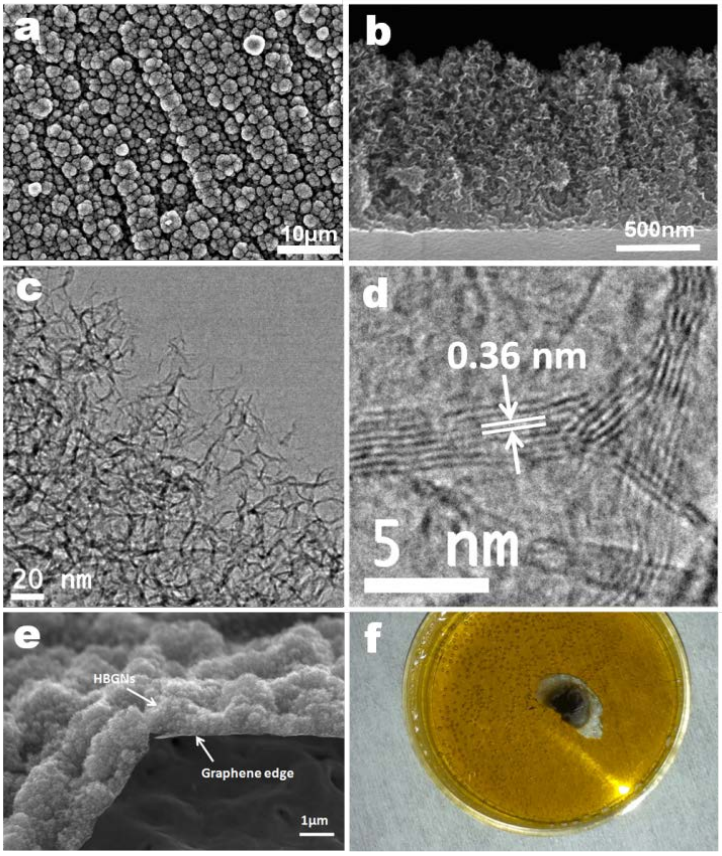

Fig. 28. SEM image of top view (a) and side view (b) of HBGNs on a graphene film on a Cu foil; granule-like HBGNs are uniformly grown on the graphene film. TEM image (c) and HRTEM image (d) of HBGNs; highly dense graphene networks with small-sized graphene sheets. (e) Tilted SEM image of HBGNs on the graphene film; the bent edge of graphene film that was peeled off from the substrate clearly shows the deposition of HBGNs on the graphene film. (f) HBGNs on the graphene film after etching Cu foil using 1M $FeCl_3$ + 1M HCl; the bright side of the rim is the graphene film without deposition of HBGNs.

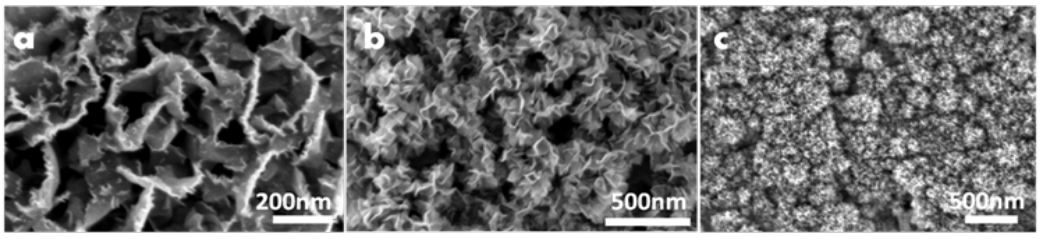

Fig. 29. Growth stage of HBGNs on the graphene film at different growth time: 5 min (a), 10 min (b), and 30 min (c). New graphene sheets with smaller domain size nucleate on the surface and edge of existing graphene sheets.

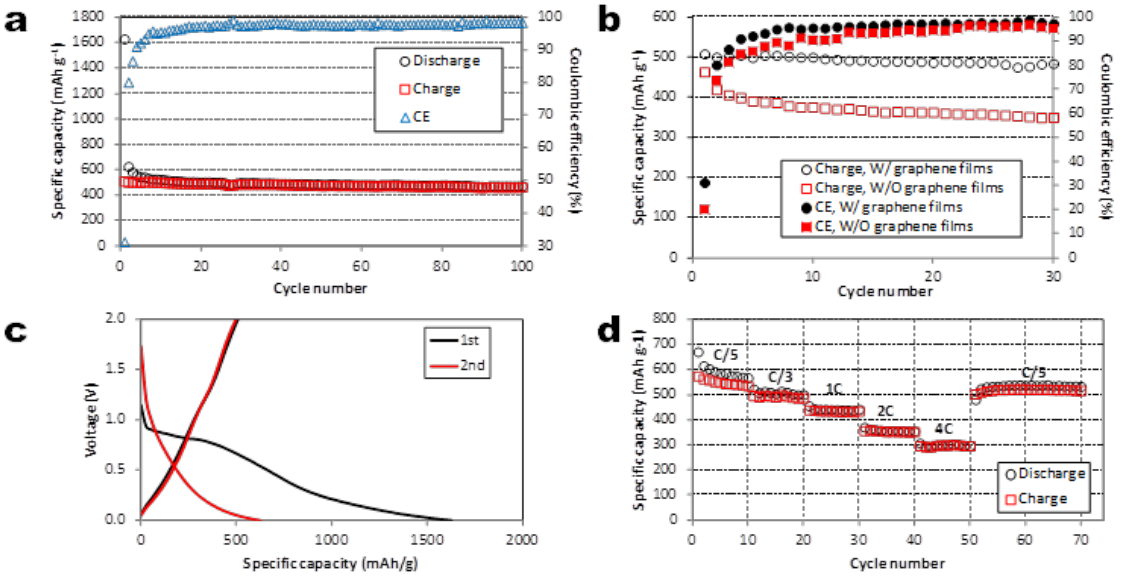

Fig. 30. (a) Cycle performance (charge, discharge, and Coulombic efficiency or CE) between 0.01 and 2.0 V at a rate of C/5 (current density of 50mA/g) for HBGNs with a graphene underlayer. (b) Comparison of the cycle performance of HBGNs electrode with and without the underlying graphene film. (c) Galvanostatic charge/discharge cycle at a current rate of C/5 in the first two cycles. (d) Rate performance of HBGNs on the graphene film at various current densities; the coin cell was cycled at C/26 in the first 3 cycles and subsequently cycled at higher current rates.

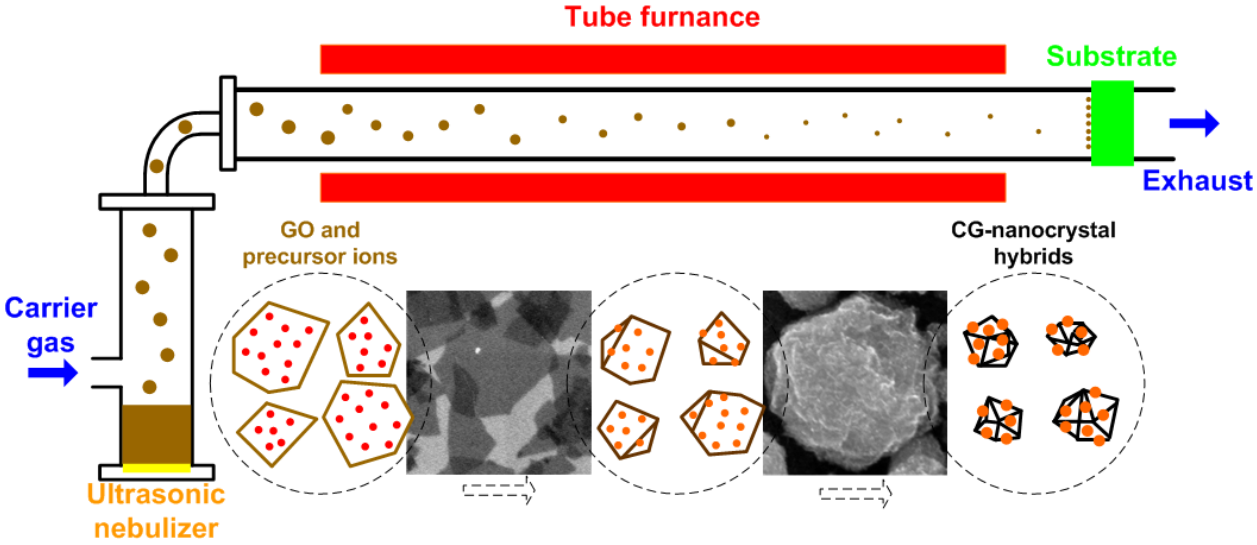

Fig. 31. Preparation of CG-nanocrystal hybrids by rapid compression of GO sheets in evaporating aerosol droplets and simultaneous chemical reactions for growth of nanocrystals on the CG surface. Schematic illustration of the experimental setup and the aerosolization/high temperature-induced GO crumpling and nanocrystal growth process.

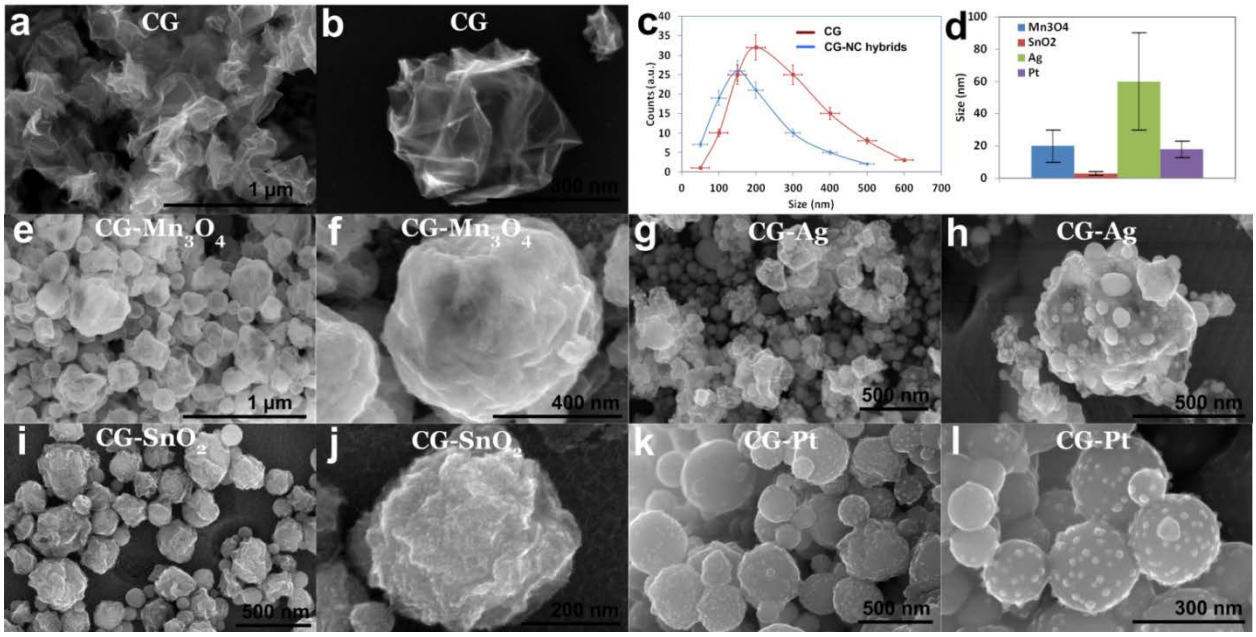

Fig. 32. SEM images of bare CG and CG-nanocrystal hybrids: a) and b) bare CG balls; e) and f) CG-Mn_3O_4 nanocrystal hybrids; g) and h) CG-Ag nanocrystal hybrids; i) and j) CG-SnO_2 nanocrystal hybrids; k) and l) CG-Pt nanocrystal hybrids. c) Size distributions of bare CG and CG-nanocrystal hybrids. d) Measured size ranges of nanocrystals from SEM and TEM images.

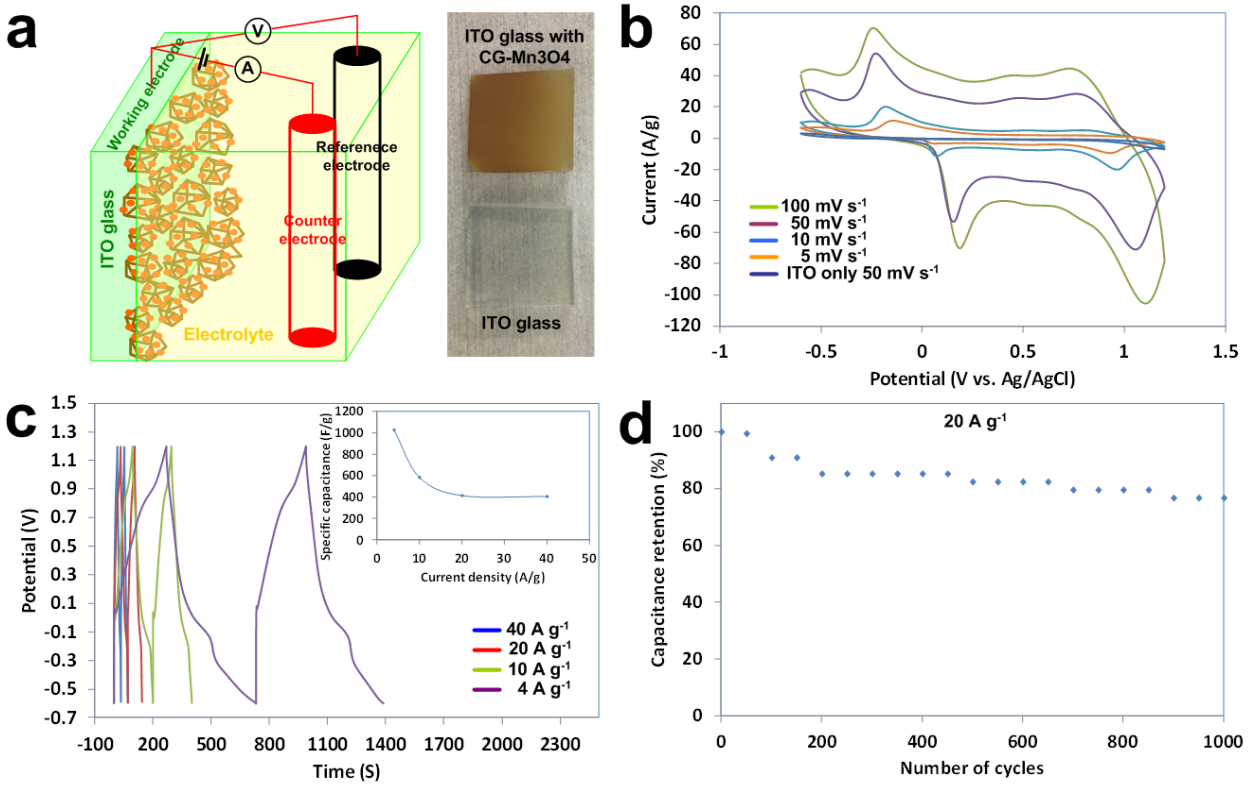

Fig. 33. a) Schematic of the capacitor test for CG-Mn_3O_4 nanocrystal hybrid electrode in a 1.0 M Na_2SO_4 aqueous electrolyte; digital pictures show the ITO glass before and after coating CG-Mn_3O_4 nanocrystal hybrids. b) Cyclic voltammograms for CG-Mn_3O_4 at different scan rates (CV curve for ITO-only at a scan rate of 50 $mV \cdot s^{-1}$ is included for comparison). c) Galvanostatic charging/discharging curves measured with different current densities for the assembled hybrid EC. The inset curve shows the calculated specific capacitance at different current densities. d) Cycling performance of hybrid ECs at a current density of 20 $A \cdot g^{-1}$.

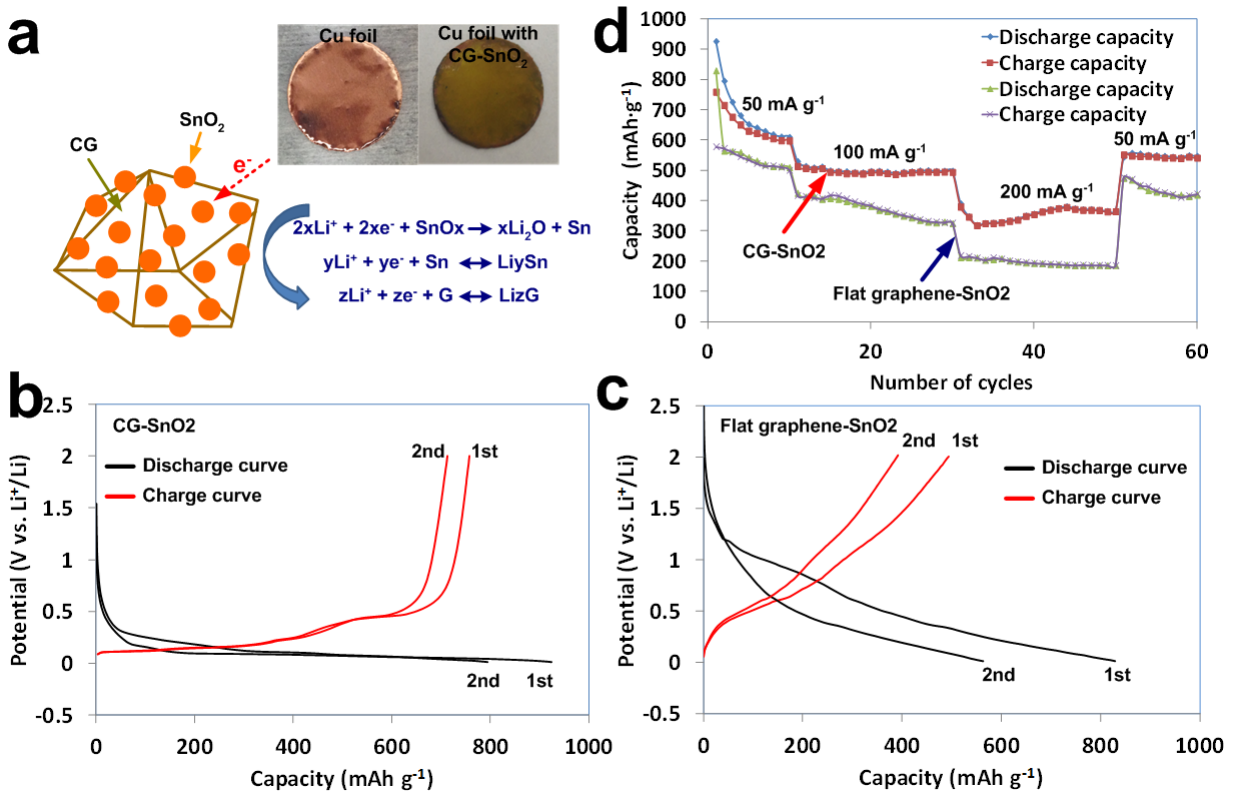

Fig. 34. a) Schematic of the LIB anode test for CG-SnO_2 nanocrystal hybrid on a copper foil. The initial two charge (red) and discharge (black) curves at a current density of 50 $mA \cdot g^{-1}$ for b) CG-SnO_2, and c) flat graphene-SnO_2. d) Capacity retention of CG-SnO_2 and flat graphene-SnO_2 at various current densities.